IEEE Access
Multidisciplinary | Rapid Review | Open Access Journal

Received August 2, 2019, accepted August 17, 2019, date of publication August 21, 2019, date of current version September 4, 2019.

Digital Object Identifier 10.1109/ACCESS.2019.2936619

Wideband Spectrum Sensing via Derived Correlation Matrix Completion Based on Generalized Coprime Sampling

KAILI JIANG, YING XIONG, AND BIN TANG

School of Information and Communication Engineering, University of Electronic Science and Technology of China, Chengdu 611731, China

Corresponding author: Kaili Jiang (jiangkelly@foxmail.com)

ABSTRACT Wideband spectrum sensing is a popular topic in signal processing, especially for many radar and communication applications. What we face is a high sampling rate and a large volume of samples, in which demand of reducing the sampling rate without sacrificing the sensing resolution and quality. The generalized coprime sampling can break the limitation of the Nyquist sampling theorem with both characteristics of sparse sensing and coprime numbers. To fully utilize all the information received of the derived correlation matrix constructed by the different time delays, the matrix completion method is exploited. The theory of matrix completion is an extension of compressive sensing, though, which is not restrained by the sparsity and the restricted isometry property. The interpolation-based method presented via the convex framework of the nuclear norm minimization has no extra fine-tuned parameters, which different from techniques like compressive covariance sampling, positive definite Toeplitz matrix completion, and so on. Moreover, compared to the selection-based method under a continuous set, the proposed method improves the spectral resolution and estimation accuracy to avoid the information losing. The Simulation results indicate the performance of the algorithm.

INDEX TERMS Wideband spectrum sensing, coprime sampling, correlation matrix completion, nuclear norm minimization, derived signal reconstruction.

I. INTRODUCTION

Advances in wideband radio-frequency (RF) technology for many radar and communication applications, the wideband spectrum sensing becomes a popular topic in signal processing. The world around us is analog in a digital world, which lies at the analog-to-digital (ADC) technology. However, because of the limitation of Shannon sampling theorem, there is a considerable gap for the sampling rate and precision of ADC, compared with the demands. In this case, though, a volume of data needs to be stored, transmitted, and processed, which contains lots of redundant information. Although it is recognized, and the Nyquist sampling theory for the case of nonuniform sampling is generalized, which states that a bandlimited signal can be perfectly reconstructed from its samples if the average sampling rate satisfies the Nyquist condition [1].

A common approach, interleaved sampling is often used for increasing the equivalent sampling rate, which presents useful not only in the temporal domain but in the frequency and spatial domain. Multi-rate sampling (MRS) and multi-coset sampling (MCS) are two sides of the time-interleaved sampling (TIS). The MCS consists of a bank of ADCs with phase delays. While the MRS also consists of a bank of ADCs but without phase delays. The typical method for resolving frequency ambiguities of the multi-rate sampled signal is based on the Chinese remainder theorem (CRT). The discrete Fourier transform (DFT) bin numbers naturally encode frequency information of the real signal into the symmetrical residues, and its dynamic range is demonstrated in [2]. Then the range of the multiple detectable frequencies for the complex signal is extended in [3]. The conclusion, according to the studies, is that the number of the different sampling rates has a linear relation with the maximum number of the estimated frequencies. Therefore it increases the number of channels and hardware costs.

Similarly, as the development of compressive sensing (CS) [4], [5] theory, the signal can be recovered perfectly under the sparse or compressible RF environment. There are series of algorithms, such as convex optimization [6],

The associate editor coordinating the review of this article and approving it for publication was Jinming Wen.

 This work is licensed under a Creative Commons Attribution 4.0 License. For more information, see http://creativecommons.org/licenses/by/4.0/

orthogonal matching pursuit (OMP) [7], least absolute shrinkage and selection operator (LASSO) [8], and so on. The practical implementation of CS is called ''analog-to-information'' (A2I) RF receiver, such as Compressive Multiplexer (CMUX) [9], Modulated Wideband Converter (MWC) [10], and Nyquist Folding Receiver (NYFR) [11], etc. However, on one side, the design of hardware based on modulated sampling is a great challenge [12]. And on the other side, the algorithms of CS are based on the linear regression techniques, which is not applicable to the higher-order statistics as the power spectrum. Therefore, compressive covariance sampling is motivated to study. The covariance matrix can be recovered without the constraint of sparse on the power spectrum under MCS [13].

It is, therefore, worth noting that coprime sampling [14] is a typical example of the MRS and sparse sampling strategy. The concept of coprime has received so much attention on the array signal processing recently, such as sparsity-based direction-of-arrival (DOA) estimation [15]–[18], the robustness of the difference coarrays [19], [20], Cramer-Rao bound [21], etc. There are many similarities between wideband spectrum sensing and sparsity-based DOA estimation, which can be used as a reference. The generalized coprime sampling scheme is discussed to obtain the compression of Toeplitz covariance matrix, as shown in [22]. Compared to the uniformly subsampling scheme and the CRT-based resolution of frequency ambiguities, spectrum estimation using coprime pair of samples improves the resolution and accuracy. The sparse Fourier transform (SFFT) [23] has the same concept, whose step of frequency bucketization is using subsampling in the time domain. After that, the coprime aliasing in the frequency domain is used to detect and resolve the collision of frequency, which remains the resolution limitation of frequency ambiguities by the CRT-based method.

The matrix reconstruction receives more attention, compared to the CS, because it is restrained by the sparsity. Moreover, matrix completion is an extension of CS theory, which completes the missing elements of a matrix instead of a vector. A significant property here is that the matrix completion problem does not obey the restricted isometry property (RIP) [24] of CS theory, which provides more applicability. In [22], the reconstructed covariance matrix only selects the continuous set of the cross-lags based on the generalized coprime sampling. However, this method does not take advantage of all the information received, which is caused by an estimation performance lose. On the other hand, the Toeplitz structure and the low-rank property of the signal received at physical array are utilized to reconstruct its covariance matrix [25], resulting in an estimation performance improvement than the non-Toeplitz method. Therefore, the missing elements of the derived signal based second-order sampled are interpolated by unclear norm minimization to completing a low-rank Toeplitz correlation matrix, which is the main contribution of this paper.

The rest of this paper is organized as follows. In section II, the coprime sampled signal model is introduced first. In section III, the derived signal is formalized by vectoring the correlation matrix, inspired by the wideband DOA estimation, and the derived correlation matrix is generalized. Then the unclear norm minimization is used for the wideband spectrum sensing. Simulation results are provided in section IV to demonstrate the effectiveness of the proposed method numerically. Finally, in section V concludes the paper.

II. COPRIME SAMPLED SIGNAL MODEL

A. NYQUIST SAMPLED SIGNAL MODEL

We make usual assumptions that a wide-sense stationary process $x(t), t \in \mathbb{R}$, which consists of multiple sinusoids confined within a bandwidth B_s. Thus, it can be represented as a complex sampled vector $x[l]$ in $\mathbb{C}^L$ with a Nyquist sampling rate $f_s = 2\,B_s$, expressed as

$$x[l] = \sum_{i=0}^{I-1} \sigma_i e^{\frac{-j2\pi l f_i}{f_s}} + n[l], \quad l = 0, 1, \ldots, L-1 \tag{1}$$

where consists of I independent frequency components f_i and magnitudes σ_i, $n[l]$ is zero-mean complex additive Gaussian white noise with the variance σ_n.

The power spectral density is the Fourier transform of its correlation function under the Wiener-Khintchine theorem, which does not need the input signal to be sparse in the frequency domain. The correlation function can be expressed by

$$r[\tau] = \mathrm{E}\left\{x[l]x^*[l-\tau]\right\}, \quad \tau = -S+1, \ldots, S+1 \tag{2}$$

in which partitioned $x[l]$ into overlapped blocks of length-S as shown in Fig. 1. The superscript $(\cdot)^*$ denotes the conjugation of a matrix, and the operator $\mathrm{E}\{\cdot\}$ denotes the statistical expectation.

Then, the correlation matrix can be estimated by averaging the available B blocks as

$$\begin{aligned}\mathbf{R}_x &= \frac{1}{B}\sum_{b=1}^{B}\mathbf{x}_b\mathbf{x}_b^H \\ &= \begin{pmatrix} \hat{r}[0] & \hat{r}[-1] & \cdots & \hat{r}[-S+2] & \hat{r}[-S+1] \\ \hat{r}[1] & \hat{r}[0] & \ddots & \vdots & \hat{r}[-S+2] \\ \vdots & \hat{r}[1] & \ddots & \hat{r}[-1] & \vdots \\ \hat{r}[S-2] & \vdots & \ddots & \hat{r}[0] & \hat{r}[-1] \\ \hat{r}[S-1] & \hat{r}[S-2] & \cdots & \hat{r}[1] & \hat{r}[0] \end{pmatrix}\end{aligned} \tag{3}$$

where $\hat{r}[\tau]$ is the estimation of the correlation function, and $\mathbf{x}_b = [x_b[0], x_b[1], \ldots, x_b[S-1]]^T$. with $x_b[l] = x[l + bG]$. The superscript $(\cdot)^H$ denotes the conjugation transpose of a matrix. The correlation matrix is a Hermitian and Toeplitz matrix. Then the spectrum can be estimated using various methods of spectral analysis, such as the multiple signal classification (MUSIC) algorithm which is typical and used in this paper.

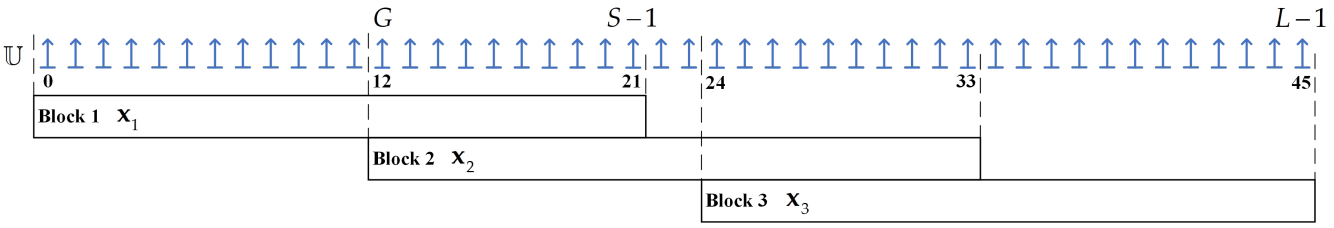

FIGURE 1. Illustration of overlapped blocks at Nyquist uniform sampling set $\mathbb{U}$.

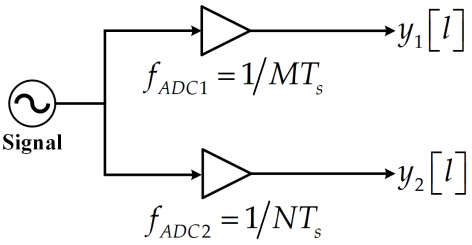

FIGURE 2. Coprime sampling scheme.

B. COPRIME SAMPLED SIGNAL MODEL

The coprime sampled signals are acquired by two channels, as presented in Fig. 2, whose sampling periods are multiples of the Nyquist sampling period and coprime. Then, the sampling instants are positioned at

$$\begin{aligned}\mathbb{U}_1 &= \{(b-1)qMNT_s + Ml_1T_s | 0 \le l_1 \le pN-1, l_1 \in \mathbb{Z}\}\\ \mathbb{U}_2 &= \{(b-1)qMNT_s + Nl_2T_s | 0 \le l_2 \le pM-1, l_2 \in \mathbb{Z}\}\end{aligned} \tag{4}$$

where $T_s = 1/f_s$ is the Nyquist sampling interval, $M \in \mathbb{N}^+$ and $N \in \mathbb{N}^+$ are coprime positive integers, $p \in \mathbb{N}^+$ is the multiple coprime unit factor and $q \in \mathbb{N}^+$ is the non-overlapping unit factor with $q \le p$, for the number of blocks $1 \le b \le B$. For illustration, an example of $M = 3$, $N = 4, p = 2, q = 1, B = 3, L = 48$ for coprime sampling scheme is presented in Figure 3.

Thus, the coprime sampled signal model can be expressed as

$$\begin{aligned}\mathbf{y}_{b1} &= \sum_{i=0}^{I-1} \sigma_i e^{\frac{-j2\pi[(b-1)qMN+Ml_1]f_i}{f_s}} + n_{b1}[l_1] = \mathbf{A}_{b1}\mathbf{\Sigma\Omega} + \mathbf{n}_{b1}\\ \mathbf{y}_{b2} &= \sum_{i=0}^{I-1} \sigma_i e^{\frac{-j2\pi[(b-1)qMN+Nl_2]f_i}{f_s}} + n_{b2}[l_2] = \mathbf{A}_{b2}\mathbf{\Sigma\Omega} + \mathbf{n}_{b2}\end{aligned} \tag{5}$$

where

$$\begin{aligned}\mathbf{\Sigma} &= \mathrm{diag}([\sigma_1, \sigma_2, \ldots, \sigma_I])_{I\times I}\\ \mathbf{A}_{b1} &= [\mathbf{a}_{b1}(f_1), \mathbf{a}_{b1}(f_2), \ldots, \mathbf{a}_{b1}(f_I)]_{pN\times I}\\ \mathbf{A}_{b2} &= [\mathbf{a}_{b2}(f_1), \mathbf{a}_{b2}(f_2), \ldots, \mathbf{a}_{b2}(f_I)]_{pM\times I}\\ \mathbf{\Omega} &= \left[a(f_1)^{-(b-1)qMN}, \ldots, a(f_I)^{-(b-1)qMN}\right]^T_{I\times 1}\\ \mathbf{n}_{b1} &\sim \mathcal{CN}\left(0, \sigma_n^2\mathbf{I}_{pN}\right), \mathbf{n}_{b2} \sim \mathcal{CN}\left(0, \sigma_n^2\mathbf{I}_{pM}\right)\end{aligned} \tag{6}$$

with

$$\begin{aligned}\mathbf{a}_{b1}(f_i) &= \left[1, a(f_i)^{-M}, a(f_i)^{-2M}, \ldots, a(f_i)^{-(pN-1)M}\right]^T_{pN\times 1}\\ \mathbf{a}_{b2}(f_i) &= \left[1, a(f_i)^{-N}, a(f_i)^{-2N}, \ldots, a(f_i)^{-(pM-1)N}\right]^T_{pM\times 1}\\ a(f_i) &= e^{j2\pi f_i/f_s}\end{aligned} \tag{7}$$

with $\mathcal{CN}(\cdot)$ denotes the complex Gaussian distribution, the superscript $(\cdot)^T$ denotes the transpose of a matrix, the operator diag$(\cdot)$ denotes diagonalization of a matrix and $\mathbf{I}$ denotes identity square matrix.

The correlation matrix can be estimated by averaging the available B blocks as

$$\begin{aligned}\mathbf{R}_{\mathbf{y}_{12}} &= \frac{1}{B}\sum_{b=1}^{B}\mathbf{y}_{b1}\mathbf{y}_{b2}^H = \mathbf{A}_{b1}\mathbf{P}\mathbf{A}_{b2}^H + \mathbf{P}_n\\ &= \sum_{i=0}^{I-1}\sigma_i^2\mathbf{a}_{b1}(f_i)\mathbf{a}_{b2}^H(f_i) + \sigma_n^2\mathbf{I}_{pN\times pM}\end{aligned} \tag{8}$$

where $\mathbf{P} = \mathrm{diag}\left(\left[\sigma_1^2, \sigma_2^2, \ldots, \sigma_I^2\right]\right)_{I\times I}$ and $\mathbf{P}_n$ denote the power square matrix of each signal and noise, respectively.

III. DERIVED CORRELATION MATRIX COMPLETION

Derived signal of second-order sampled is reconstructed by stacking columns of the correlation matrix $\mathbf{R}_{\mathbf{y}_{12}}$ sequentially into a vector $\mathbf{z}$, expressed as

$$\mathbf{z} = \mathrm{vec}\left(\mathbf{R}_{\mathbf{y}_{12}}\right) \tag{9}$$

which is the sensing of signal power with time delays as an independent variable. The operator vec$(\cdot)$ denotes vectorization of a matrix.

The difference set is formed by different time delays, as follows

$$\mathbb{D} = \{\tau | \tau = \pm(Ml_1 - Nl_2)T_s\} \tag{10}$$

which is shown in Fig. 4. Without loss of generality, assume that $M < N$, then the extremum is $\pm M(pN-1)$ and the first pair of holes are located at $\pm[(p-1)MN + M + N]$. Through selecting and averaging all the elements with the same delay τ, the derived signal through temporal smoothing is defined as

$$\langle\mathbf{z}_{\mathbb{D}}\rangle_\tau = \frac{1}{|\mathbb{D}|}\sum_{\tau\in\mathbb{D}}\langle\mathbf{z}\rangle_\tau \tag{11}$$

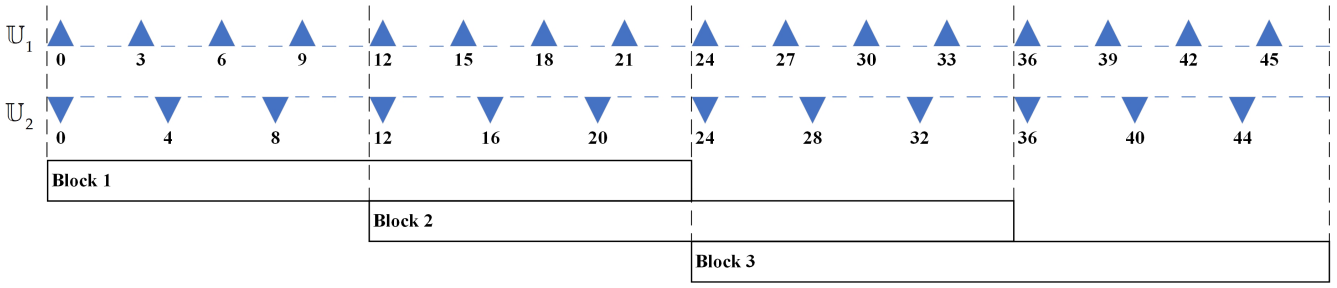

FIGURE 3. An example of $M = 3, N = 4, p = 2, q = 1, B = 3, L = 48$ for coprime sampling scheme.

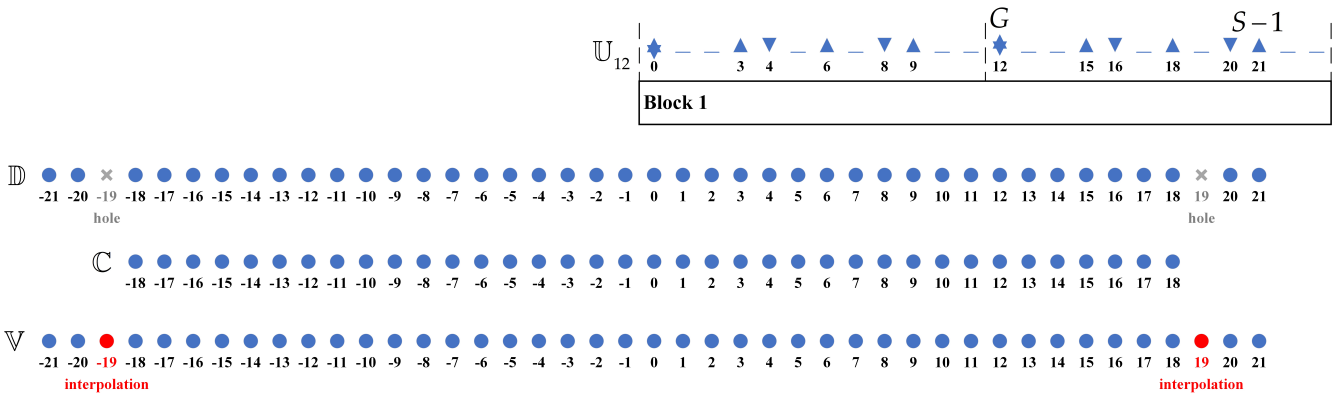

FIGURE 4. Illustration of difference set $\mathbb{D}$, continuous set $\mathbb{C}$ and virtual set $\mathbb{V}$.

where the operator $|\cdot|$ denotes the cardinality of a set, and $\langle\cdot\rangle_\tau$ denotes the element corresponding to the delay at τ.

Then, its manifold matrix can be expressed as

$$\mathbf{A}_{\mathbb{D}} = [\mathbf{a}_{\mathbb{D}}(f_1), \mathbf{a}_{\mathbb{D}}(f_2), \ldots, \mathbf{a}_{\mathbb{D}}(f_I)]_{|\mathbb{D}|\times I} \tag{12}$$

where the $|\mathbb{D}|-$by-1 vector $\mathbf{a}_{\mathbb{D}}(f_i)$ is defined as

$$\langle \mathbf{a}_{\mathbb{D}}(f_i)\rangle_\tau = a(f_i)^{-\tau}, \quad \tau \in \mathbb{D} \tag{13}$$

The continuous uniform sampled derived signal is

$$\langle \mathbf{z}_{\mathbb{C}}\rangle_\tau = \langle \mathbf{z}_{\mathbb{D}}\rangle_\tau, \quad \tau \in \mathbb{C} \tag{14}$$

which selects the elements between the first pair of holes, then the continuous set is expressed as

$$\mathbb{C} = \{\tau | \tau = \pm lT_s, 0 \le l < (p-1)MN + M + N, l \in \mathbb{Z}\} \tag{15}$$

Thus, the derived correlation matrix can be acquired by

$$\mathbf{R}_{\mathbf{z}_{\mathbb{C}}} = \begin{bmatrix} \langle \mathbf{z}_{\mathbb{C}}\rangle_{\frac{(|\mathbb{C}|+1)}{2}} & \langle \mathbf{z}_{\mathbb{C}}\rangle_{\frac{(|\mathbb{C}|+1)}{2}-1} & \cdots & \langle \mathbf{z}_{\mathbb{C}}\rangle_1 \\ \langle \mathbf{z}_{\mathbb{C}}\rangle_{\frac{(|\mathbb{C}|+1)}{2}+1} & \langle \mathbf{z}_{\mathbb{C}}\rangle_{\frac{(|\mathbb{C}|+1)}{2}} & \cdots & \langle \mathbf{z}_{\mathbb{C}}\rangle_2 \\ \vdots & \vdots & \ddots & \vdots \\ \langle \mathbf{z}_{\mathbb{C}}\rangle_{|\mathbb{C}|} & \langle \mathbf{z}_{\mathbb{C}}\rangle_{|\mathbb{C}|-1} & \cdots & \langle \mathbf{z}_{\mathbb{C}}\rangle_{\frac{(|\mathbb{C}|+1)}{2}} \end{bmatrix} \tag{16}$$

The resolution of power spectrum can be given as $S_{\mathbf{z}_{\mathbb{C}}} = (p-1)MN + M + N - 1$ by spectral analyzing. Because of the holes of difference set, the part information of $\mathbf{z}_{\mathbb{D}}$ is not used. Therefore, to utilizing the information of $\mathbf{z}_{\mathbb{D}}$ entirely, for increasing the resolution of the power spectrum, with the low-rank property and Toeplitz structure of the correlation matrix, interpolating zero-value in the position of missing elements. Then, the problem of interpolation can be changed into a matrix completion problem.

Selecting the elements between extremum of difference set, and interpolating zero-value in holes, defined as a virtual set

$$\mathbb{V} = \{\tau | \tau = \pm lT_s, 0 \le l \le M(pN-1), l \in \mathbb{Z}\} \tag{17}$$

The derived virtual signal corresponding is

$$\langle \mathbf{z}_{\mathbb{V}}\rangle_\tau = \begin{cases} \langle \mathbf{z}_{\mathbb{D}}\rangle_\tau, & \tau \in \mathbb{D} \\ 0, & \tau \in \mathbb{V} - \mathbb{D} \end{cases} \tag{18}$$

which is uniform and continuous. Nevertheless, the difference between Nyquist sampled, there is zero-value of the hole position. Thus, define a binary index vector $\mathbf{g}_{\mathbb{V}}$ as

$$\langle \mathbf{g}_{\mathbb{V}}\rangle_\tau = \begin{cases} 1, & \tau \in \mathbb{D} \\ 0, & \tau \in \mathbb{V} - \mathbb{D} \end{cases} \tag{19}$$

where zero-value and one-value elements denote whether or not missing elements of delays. Then, we can get

$$\mathbf{z}_{\mathbb{V}} = \mathbf{z}_{\mathbb{U}} \odot \mathbf{g}_{\mathbb{V}} \tag{20}$$

where $\mathbf{z}_{\mathbb{U}}$ denotes the vector of correlation function from Nyquist sampling, and the operator $\odot$ denotes the Hadamard product operator.

Therefore, the derived virtual correlation matrix can be recovered by solving the matrix rank minimization problem as

$$\begin{aligned} \min \quad & \operatorname{rank}\left(\mathbf{R}_{\mathbf{z}_{\mathbb{V}}}\right) \\ \text{subject to } & \mathbf{R}_{\mathbf{z}_{\mathbb{V}}} \odot \mathbf{G} = \mathbf{R}_{\mathbf{z}_{\mathbb{D}}} \\ & \mathbf{R}_{\mathbf{z}_{\mathbb{V}}} = \mathbf{R}_{\mathbf{z}_{\mathbb{V}}}^{H} \end{aligned} \tag{21}$$

where $\mathbf{G} = \mathbf{g}_{\mathbb{V}}\mathbf{g}_{\mathbb{V}}^{T}$, and the operator rank$(\cdot)$ denotes the rank of a matrix.

This analogous to ℓ_0-norm minimization problem in the CS theory, which is an NP-hard problem and cannot be solved exactly. Just as ℓ_1-norm minimization is the tightest convex relaxation of the ℓ_0-norm minimization problem, the NP-hard rank minimization problem turns into a nuclear norm minimization as

$$\begin{aligned} \min \quad & \left\|\mathbf{R}_{\mathbf{z}_{\mathbb{V}}}\right\|_{*} \\ \text{subject to } & \mathbf{R}_{\mathbf{z}_{\mathbb{V}}} \odot \mathbf{G} = \mathbf{R}_{\mathbf{z}_{\mathbb{D}}} \\ & \mathbf{R}_{\mathbf{z}_{\mathbb{V}}} = \mathbf{R}_{\mathbf{z}_{\mathbb{V}}}^{H} \end{aligned} \tag{22}$$

where the symbol $\|\cdot\|_{*}$ denotes nuclear norm of a matrix. This problem can be solved by CVX package [6]. Then, the resolution of the power spectrum increases up to $S_{\mathbf{z}_{\mathbb{V}}} = M(pN-1)$ though the conventional methods of spectral analyzing, which is the same as Nyquist sampling of length-S blocks.

IV. SIMULATION RESULTS

In this section, the numerical examples show the spectrum sensing performance of the derived correlation matrix completion method. Assume that I independent frequency components of the inputs are distributed in the frequency band $[-0.5, 0.5)$ GHz, with magnitudes $\sigma_i = 1$ for $i = 1, 2, \ldots, I$. And the noise power is assumed to be identical across the entire spectrum. Meanwhile, assume there are $L = 30000$ uniform samples generated by the Nyquist sampling rate $f_s = 1$GHz. The coprime pair $M = 3$ and $N = 4$ are set in the following simulation, because of the optimal coprime pair should as close as possible in terms of total samples [22]. Besides, $p = 2$ and $q = 1$ are used to illustrate the performance of the frequencies identification, as shown in Fig. 5, where the input signal-to-noise ratio (SNR) is set to -10 dB. Afterwards, the relative root mean square error (Relative RMSE) of the estimated frequencies [22] is adopted to evaluate the performance, defined as

$$\text{Relative RMSE}\,(f_i) = \frac{1}{f_s}\sqrt{\frac{1}{500I}\sum_{k=1}^{500}\sum_{i=1}^{I}\left(\hat{f}_i(k) - f_i\right)^2} \tag{23}$$

where $\hat{f}_i(k)$ is the estimation of f from the k-th Monte Carlo trial.

The correlation matrix $\mathbf{R}_{\mathbf{z}_{\mathbb{C}}}$ and $\mathbf{R}_{\mathbf{z}_{\mathbb{V}}}$ can be reconstructed from $\mathbf{R}_{\mathbf{y}_{12}}$, with the dimensions are compressed from $\left(S_{\mathbf{z}_{\mathbb{C}}}+1\right)$-by-$\left(S_{\mathbf{z}_{\mathbb{C}}}+1\right) = 19$-by-$19$ and $\left(S_{\mathbf{z}_{\mathbb{V}}}+1\right)$-by-$\left(S_{\mathbf{z}_{\mathbb{V}}}+1\right) = 22$-by-$22$ to $pM \times pN = 6\times 8$. Thus, the resulting compression factor is improved from 7.52 to 10.08, and the maximum number of distinguishable frequencies up to $S_{\mathbf{z}_{\mathbb{V}}} = 21$. In Fig. 5, we consider $I = 21$ independent frequency components which are selected in the frequency band uniformly. All the 21 frequencies are identified correctly under virtual set $\mathbb{V}$, as shown in Fig. 5(b), with the RMSE $= 0.0035$. While there are only 18 frequencies are identified under the continuous set $\mathbb{C}$, as shown in Fig. 5(a), with the RMSE $= 0.0284$. The reason for this is that the number of frequencies to be estimated exceeds the dimension limited under the continuous set $\mathbb{C}$.

Moreover, according to the CRT-based method, there are two frequencies at most can be uniquely determined by the equivalent Nyquist sampling rate $\max\{1/MT_s, 1/NT_s\} = 0.25\ f_s$, while the range can be extended to $\operatorname{lcm}\left\{1/MT_s, 1/NT_s\right\} \approx 0.58\ f_s$ for the single-frequency estimation.

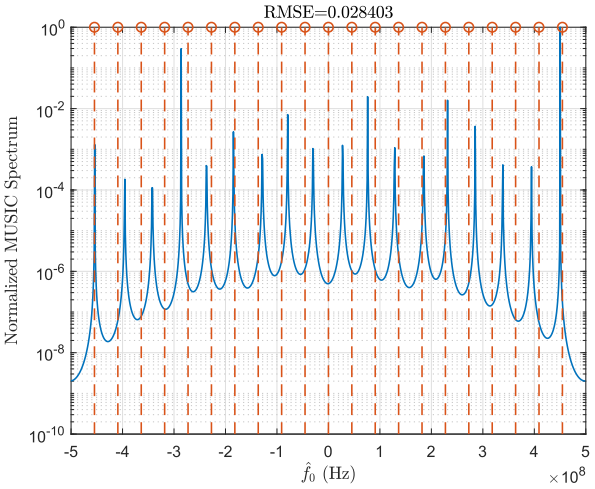

(a) Continuous set $\mathbb{C} \in \{-18, -17, \ldots, 0, \ldots, 17, 18\}$

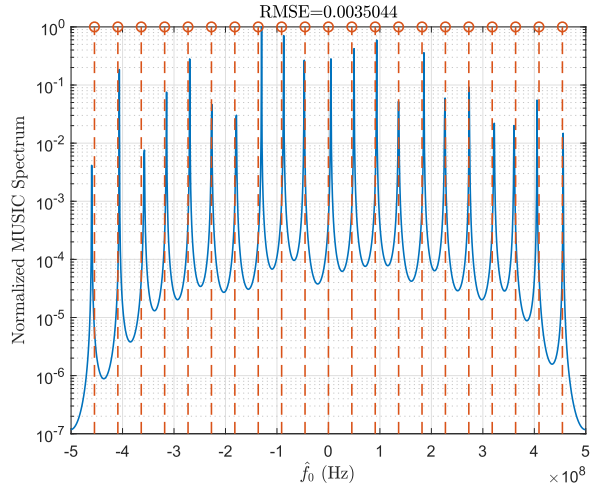

(b) Virtual set $\mathbb{V} \in \{-21, -20, \ldots, 0, \ldots, 20, 21\}$

FIGURE 5. The normalized MUSCI spectrum is estimated under continuous set C and virtual set V.

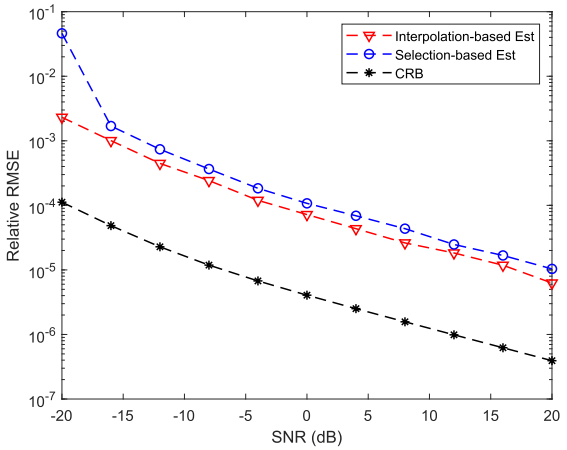

FIGURE 6. Relative RMSE versus SNR ($I = 1$).

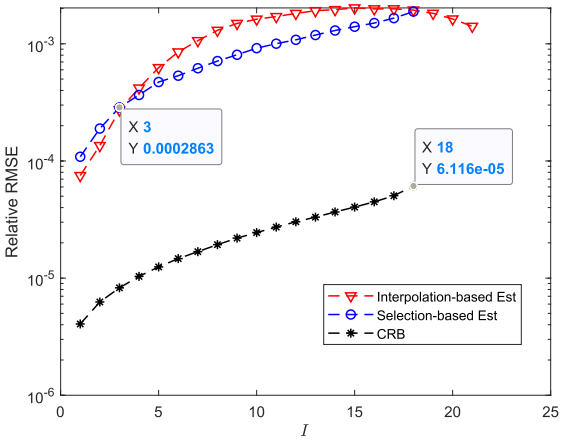

FIGURE 7. Relative RMSE versus I (SNR = 0 dB).

On the other hand, the generalized coprime sampling can be cast into the CS framework, whose sensing matrix is the partial IDFT. Based on the RIP of CS theory, the required number of samples for the sensing matrices should satisfy $p(M+N-1) > I\ln S$, whose rows of the measurement matrix are chosen uniformly at random [26]. Thus, under the same condition as Fig. 5, $I < 3.88$ different frequencies can be recovered with high probability. Therefore, compared to the two method mentioned above, we can see the advantage of the proposed method on improving the spectral resolution.

In Fig. 6, the Relative RMSE results under continuous set $\mathbb{C}$ and virtual set $\mathbb{V}$ are compared as a function of the input SNR, where $I = 1$ is assumed. And the Cramer-Rao bounds (CRB) for sparse sampling in the context of array processing [21] can be a reference to the frequency estimation when more inputs than the number of samples.

For the outputs $\mathbf{y}_b = [\mathbf{y}_{b1}^T\ \mathbf{y}_{b2}^T]^T, b = 1, 2, \ldots, B$ which stact all the coprime samples, the CRB is the inverse of the Fisher information matrix (FIM) for the parameter vector $\boldsymbol{\alpha} = [\mathbf{f}^T, \boldsymbol{\sigma}^T]^T$, where $\mathbf{f} = [f_1/f_s, f_2/f_s, \ldots, f_I/f_s]^T$ is the normalized frequencies and $\boldsymbol{\sigma} = [\sigma_1, \sigma_2, \ldots, \sigma_I, \sigma_n]^T$. And the elements of the FIM can be expressed as

$$F_{i,j} = B\ \mathrm{tr}\{\mathbf{R_y}^{-1}\frac{\partial \mathbf{R_y}}{\partial \alpha_i}\mathbf{R_y}^{-1}\frac{\partial \mathbf{R_y}}{\partial \alpha_j}\} \tag{24}$$

where the operator $\mathrm{tr}\{\cdot\}$ is the trace of a matrix and $\mathbf{R_y}$ is

$$\mathbf{R_y} = \mathrm{E}\{\mathbf{y}_b\mathbf{y}_b^H\} = \sum_{i=0}^{I-1}\sigma_i^2\mathbf{a}_b(f_i)\mathbf{a}_b^H(f_i) + \sigma_n^2\mathbf{I}_{p(M+N)} \tag{25}$$

and $\mathbf{a}_b(f_i) = [\mathbf{a}_{b1}^T(f_i)\ \mathbf{a}_{b2}^T(f_i)]^T$.

Recall the proof from appendix A.4 in [21], the closed-form expression for the normalized frequencies can be rewritten as

$$\mathrm{CRB}(\mathbf{f}) = \frac{1}{4\pi^2 B}\left(\mathbf{G}_0^H\,\boldsymbol{\Pi}^{\perp}_{\mathbf{MW}_{\mathbb{D}}}\mathbf{G}_0\right)^{-1} \tag{26}$$

which is valid under the rank condition $\mathrm{rank}\,(\mathbf{A}_{\mathrm{ACM}}) = 2I+1$ based on the difference set, where $\mathbf{A}_{\mathrm{ACM}} = \left[\mathrm{diag}(\mathbb{D})\mathbf{A}_{\mathbb{D}}\ \mathbf{W}_{\mathbb{D}}\right]$ with $\mathbf{W}_{\mathbb{D}} = [\mathbf{A}_{\mathbb{D}}\ \mathbf{e}_0]$ and $\mathbf{e}_0$ is a column vector with one in middle and zero elsewhere. Meanwhile, the other parameters are as follows

$$\begin{aligned}\mathbf{G}_0 &= \mathbf{M}(\mathrm{diag}(\mathbb{D}))\mathbf{A}_{\mathbb{D}}\mathbf{P}\\ \mathbf{M} &= \left(\mathbf{J}^H\left(\mathbf{R_y}\otimes\mathbf{R_y}\right)^{-1}\mathbf{J}\right)^{\frac{1}{2}}\end{aligned} \tag{27}$$

where the operator $\boldsymbol{\Pi}^{\perp}_{\mathbf{A}} = \mathbf{I} - \mathbf{A}(\mathbf{A}^H\mathbf{A})^{-1}\mathbf{A}^H$, and $\mathbf{J}$ is a binary index matrix with size $|z|-\mathrm{by}-|\mathbb{D}|$, whose column with different time delays τ is given by

$$\langle\mathbf{J}\rangle_{:\tau} = \mathrm{vec}(\mathbf{I}(\tau)), \quad \tau \in \mathbb{D} \tag{28}$$

where the $|z|-\mathrm{by}-|z|$ matrix $\mathbf{I}(\tau)$ satisfies

$$\langle\mathbf{I}(\tau)\rangle_{l_1,l_2} = \begin{cases}1, & \text{if } l_1 - l_2 = \tau\\ 0, & \text{otherwise},\end{cases} \quad l_1, l_2 \in \mathbb{U}_1 \cup \mathbb{U}_2 \tag{29}$$

with $|z| = p(M+N)$.

We can see that all of them display a strong inverse semi-logarithmic dependence on the input SNR, the same as shown in [22]. The performance of the interpolation-based method under virtual set $\mathbb{V}$ is a little better than the selection-based method under continuous set $\mathbb{C}$. That is because the selection-based method only adopts the consecutive parts of the difference set. In addition, the gap between the Relative RMSE and CRB comes from the reconstruction error. The reconstruction error increase with the number of frequency components, as we can see from Fig. 7, where the input SNR is set to 0 dB. When the number of estimated frequencies is less than four, the performance of the interpolation-based method under virtual set $\mathbb{V}$ is a little better than the selection-based method under continuous set $\mathbb{C}$. As a result, the same conclusion has been obtained based on the RIP analysis of CS theory, that $I < 3.88$ different frequencies can be recovered with high probability. In addition, the CRB expression is divergent when $I > 18$, since the rank condition matrix $\mathbf{A}_{\mathrm{ACM}}$ does not have full column rank.

In Fig. 8, we present the Relative RMSE and CRB results versus different p for $q = 1$, where $I = 5$ frequencies

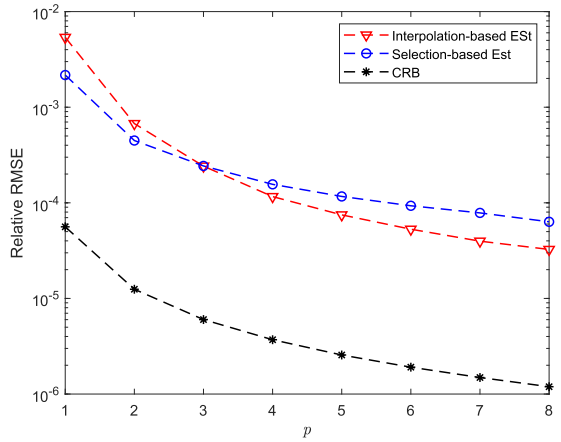

FIGURE 8. Relative RMSE versus p ($q = 1$, $I = 5$).

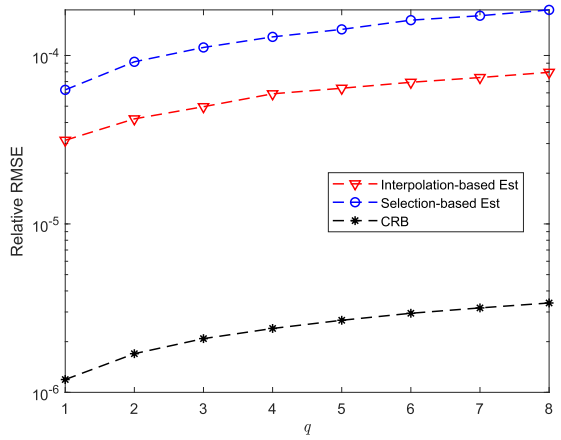

FIGURE 9. Relative RMSE versus q ($p = 8$, $I = 5$).

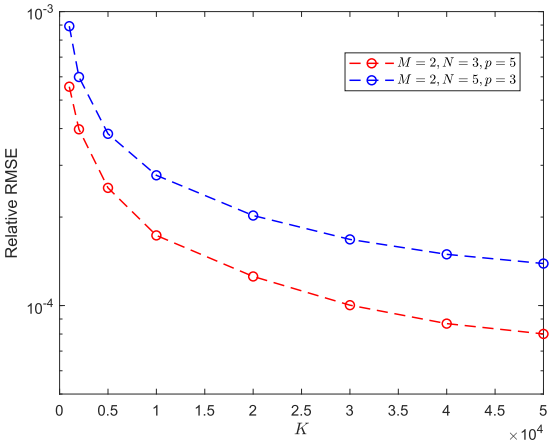

FIGURE 10. Relative RMSE versus K with the same resolution $S_{\mathbf{z}_{\mathbb{V}}} = 28$ ($I = 5$).

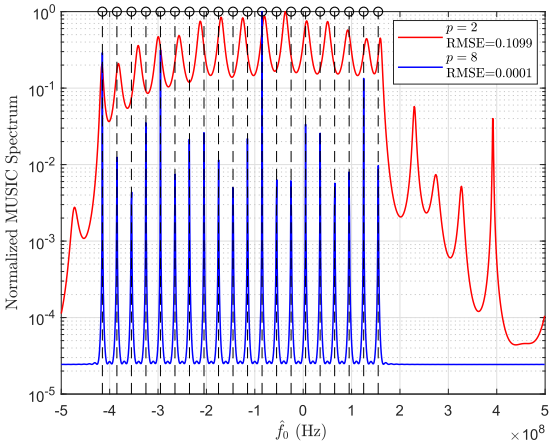

FIGURE 11. The normalized MUSCI spectrum is estimated for the cases of $p = 2$ and $p = 8$ ($q = 1$, $I = 20$).

are assumed, with the 0dB SNR. It is clear that the estimation accuracy is improved as p increases. The observed improvement in the Relative RMSE and CRB is attributed to the number of different time delays increases with p. In other words, there is a higher spectral resolution and estimation accuracy under the same inputs, with higher storage and computation. In addition, the gap between the Relative RMSE and CRB becomes smaller in the interpolation-based than in the selection-based. The result can be explained by the RIP that $I = 5$ is selected in this part, due to the resulting number of estimated frequencies $I < \{2.73, 3.94, 5.15, 6.30, 7.42, 8.50, 9.56, 10.59\}$ based on the different choices of $p(M + N - 1) > I \ln S$.

In Fig. 9, similarly, we present the Relative RMSE results and CRB versus different q for $p = 8$, where $I = 5$ frequencies are assumed, with the 0dB SNR. It is clear that estimation accuracy is improved as q decreases. The observed improvement in the Relative RMSE and CRB is attributed to the number of overlapping blocks increases with the decrease of q. There is a similar conclusion in Fig. 10, obviously, that the estimation performance is improved as the number of samples K increases, due to the higher resulting number of overlapping blocks to smoothing noise. However, for the same spectral resolution $S_{\mathbf{z}_{\mathbb{V}}} = 28$ and $M = 2$, the observed decreases in the estimated Relative RMSE with the increasing of N is attributed to more nonuniform samples are introduced. In Fig. 11, the normalized MUSIC spectrum is estimated for the cases of $p = 2$ and $p = 8$, where $I = 20$ frequencies from -415 MHz to 155 MHz are considered with 30 MHz separation under the 0 dB SNR. Although the resolution $S_{\mathbf{z}_{\mathbb{V}}} = 21$ of the case of $p = 2$ is higher than the frequencies to be estimated, but the performance is poor than the case of $p = 8$ for the case of frequencies distributed nonuniformly throughout the detection range.

V. CONCLUSION

The derived correlation matrix completion method for generalized coprime sampling is proposed as an interpolation-based strategy. Being an extension of CS theory, the algorithm of matrix completion is not restrained by the RIP. The derived correlation matrix completion based on the nuclear norm minimization not only has no extra fine-tuned parameters, but also improves spectral resolution compared

to the CS-based and CRT-based algorithms. Meanwhile, the improved spectral resolution and estimation accuracy can be obtained compared to the selection-based strategy, due to utilizing all the information received, which is verified in the simulation part.

REFERENCES

[1] M. Mishali and Y. C. Eldar, "Sub-Nyquist sampling," *IEEE Signal Process. Mag.*, vol. 28, no. 6, pp. 98–124, Nov. 2011.
[2] P. E. Pace, P. Stănică, B. L. Luke, and T. W. Tedesso, "Extended closed-form expressions for the robust symmetrical number system dynamic range and an efficient algorithm for its computation," *IEEE Trans. Inf. Theory*, vol. 60, no. 3, pp. 1742–1752, Mar. 2014.
[3] L. Xiao and X.-G. Xia, "Frequency determination from truly sub-Nyquist samplers based on robust Chinese remainder theorem," *Signal Process.*, vol. 150, pp. 248–258, Sep. 2018.
[4] S. Sharma, A. Gupta, and V. Bhatia, "A new sparse signal-matched measurement matrix for compressive sensing in UWB communication," *IEEE Access*, vol. 4, pp. 5327–5342, 2016.
[5] Y. Arjoune, N. Kaabouch, H. El Ghazi, and A. Tamtaoui, "A performance comparison of measurement matrices in compressive sensing," *Int. J. Commun. Syst.*, vol. 31, no. 10, Jul. 2018, Art. no. e3576.
[6] M. Grant and S. Boyd. (2014). *CVX: MATLAB Software for Disciplined Convex Programming, Version 2.1*. [Online]. Available: http://cvxr.com/cvx
[7] J. Wang and B. Shim, "On the recovery limit of sparse signals using orthogonal matching pursuit," *IEEE Trans. Signal Process.*, vol. 60, no. 9, pp. 4973–4976, Sep. 2012.
[8] R. Tibshirani, "Regression shrinkage and selection via the lasso: A retrospective," *J. Roy. Stat. Soc., B (Stat. Methodol.)*, vol. 73, no. 3, pp. 273–282, Jun. 2011.
[9] J. P. Slavinsky, J. N. Laska, M. A. Davenport, and R. G. Baraniuk, "The compressive multiplexer for multi-channel compressive sensing," in *Proc. IEEE Int. Conf. Acoust., Speech Signal Process. (ICASSP)*, Prague, Czech Republic, May 2011, pp. 3980–3983.
[10] M. Mishali, Y. C. Eldar, and A. J. Elron, "Xampling: Signal acquisition and processing in union of subspaces," *IEEE Trans. Signal Process.*, vol. 59, no. 10, pp. 4719–4734, Oct. 2011.
[11] R. Maleh, G. L. Fudge, F. A. Boyle, and P. E. Pace, "Analog-to-information and the Nyquist folding receiver," *IEEE J. Emerg. Sel. Topics Circuits Syst.*, vol. 2, no. 3, pp. 564–578, Sep. 2012.
[12] T. Strohmer, "Measure what should be measured: Progress and challenges in compressive sensing," *IEEE Signal Process. Lett.*, vol. 19, no. 12, pp. 887–893, Dec. 2012.
[13] D. D. Arianandа and G. Leus, "Compressive wideband power spectrum estimation," *IEEE Trans. Signal Process.*, vol. 60, no. 9, pp. 4775–4789, Sep. 2012.
[14] P. P. Vaidyanathan and P. Pal, "Sparse sensing with co-prime samplers and arrays," *IEEE Trans. Signal Process.*, vol. 59, no. 2, pp. 573–586, Feb. 2011.
[15] S. Qin, Y. D. Zhang, and M. G. Amin, "Generalized coprime array configurations for direction-of-arrival estimation," *IEEE Trans. Signal Process.*, vol. 63, no. 6, pp. 1377–1390, Mar. 2015.
[16] C. Zhou, Y. Gu, Z. Shi, and Y. D. Zhang, "Off-grid direction-of-arrival estimation using coprime array interpolation," *IEEE Signal Process. Lett.*, vol. 25, no. 11, pp. 1710–1714, Nov. 2018.
[17] C. Zhou, Y. Gu, X. Fan, Z. Shi, G. Mao, and Y. D. Zhang, "Direction-of-arrival estimation for coprime array via virtual array interpolation," *IEEE Trans. Signal Process.*, vol. 66, no. 22, pp. 5956–5971, Nov. 2018.
[18] G. Qin, M. G. Amin, and Y. D. Zhang, "DOA estimation exploiting sparse array motions," *IEEE Trans. Signal Process.*, vol. 67, no. 11, pp. 3013–3027, Jun. 2019.
[19] C.-L. Liu and P. P. Vaidyanathan, "Robustness of difference coarrays of sparse arrays to sensor failures—Part I: A theory motivated by coarray MUSIC," *IEEE Trans. Signal Process.*, vol. 67, no. 12, pp. 3213–3226, Jun. 2019.
[20] C.-L. Liu and P. P. Vaidyanathan, "Robustness of difference coarrays of sparse arrays to sensor failures—Part II: Array geometries," *IEEE Trans. Signal Process.*, vol. 67, no. 12, pp. 3227–3242, Jun. 2019.
[21] C.-L. Liu and P. P. Vaidyanathan, "Cramér–Rao bounds for coprime and other sparse arrays, which find more sources than sensors," *Digit. Signal Process.*, vol. 61, pp. 43–61, Feb. 2017.
[22] S. Qin, Y. D. Zhang, M. G. Amin, and A. M. Zoubir, "Generalized coprime sampling of toeplitz matrices for spectrum estimation," *IEEE Trans. Signal Process.*, vol. 65, no. 1, pp. 81–94, Jan. 2017.
[23] H. Hassanieh, L. Shi, O. Abari, E. Hamed, and D. Katabi, "GHz-wide sensing and decoding using the sparse Fourier transform," in *Proc. IEEE INFOCOM-IEEE Conf. Comput. Commun.*, Toronto, ON, Canada, Apr./May 2014, pp. 2256–2264.
[24] E. J. Candès and Y. Plan, "Matrix completion with noise," *Proc. IEEE*, vol. 98, no. 6, pp. 925–936, Jun. 2010.
[25] X. Wu, W.-P. Zhu, and J. Yan, "A Toeplitz covariance matrix reconstruction approach for direction-of-arrival estimation," *IEEE Trans. Veh. Technol.*, vol. 66, no. 9, pp. 8223–8237, Sep. 2017.
[26] R. Calderbank, S. Howard, and S. Jafarpour, "Construction of a large class of deterministic sensing matrices that satisfy a statistical isometry property," *IEEE J. Sel. Topics Signal Process.*, vol. 4, no. 2, pp. 358–374, Apr. 2010.

KAILI JIANG received the B.S. degree from the University of Electronic Science and Technology of China, Chengdu, China, in 2013, where she is currently pursuing the Ph.D. degree with the School of Information and Communication Engineering. Her research interests include wideband spectrum sensing, sparse/compressive sensing, and radar signal processing.

YING XIONG is currently a Professor with the School of Information and Communication Engineering, University of Electronic Science and Technology of China, Chengdu, China. Her research interests include radar reconnaissance, interference, and countermeasure technology for the low probability of intercept radar signal and the broadband/ultra-wideband radar signal.

BIN TANG is currently a Professor with the School of Information and Communication Engineering, University of Electronic Science and Technology of China, Chengdu, China. His research interests include the low probability of intercept radar signal processing, adaptive radar reconnaissance and interference technology, networked radar countermeasure technology, and broadband/ultra-wideband radar digital reconnaissance receiving and interference technology.